

Galactic Wind in NGC 4460: New Observations

D.V. Oparin^{1*} and A.V. Moiseev^{2***}

¹Special Astrophysical Observatory, Russian Academy of Sciences, Nizhnij Arkhyz, 369167, Russia

²Sternberg Astronomical Institute, M.V. Lomonosov Moscow State University, Universitetsky pr., 13, Moscow, 119991

May 19, 2015/Revised: July 31, 2015

Abstract. NGC 4460 is an isolated lenticular galaxy, in which galactic wind has been earlier discovered as a gas outflow associated with circumnuclear regions of star formation. Using the results of observations in the H α line with the scanning Fabry–Perot interferometer on the SAO RAS 6-m telescope, we studied the kinematics of the ionized gas in this galaxy. The parameters of gas outflow from the plane of the galactic disk were refined within a simple geometric model. We show that it is impossible to characterize the wind by a fixed velocity value. Characteristic outflow velocities are within 30–80 km s^{−1}, and they are insufficient to make the swept-out matter ultimately leave the galaxy.

1. Introduction

Galactic wind (galactic outflow, superwind, hereafter GW) is one of the most impressive and large-scale manifestations of the effect star formation has on the interstellar and even intergalactic medium. It looks like a stream of gas (ionized, neutral, molecular) emitted from a galaxy as a result of collective action of the phenomena related to young stellar groups: radiation pressure, winds of giant stars, supernova explosions. GW has a serious impact on the structure and chemical composition of the interstellar medium and mass distribution therein, stirring it, transferring the kinetic energy, and starting the processes of star formation (see, e.g., Veilleux et al., 2005). The results of numerical calculations underline the importance of the GW role in galactic evolution (Hopkins et al., 2012), which is also confirmed by the observations of GW manifestations among the galaxies at large redshifts (Pettini et al., 1998). The observations of galaxies with intense star formation show that the galactic outflow manifests itself in almost every one of them in one way or another, at least as a broad pedestal at the base of emission lines (Arribas et al., 2014).

Therefore, the GW phenomenon is well known (see the review of Veilleux et al., 2005) and references to yet earlier studies therein). At the same time, a detailed study of emissive nebulae, created by GW, with quite a high spatial resolution was performed only for a few nearby galaxies, such as M 82 (Westmoquette et al., 2009), NGC 253 (Matsubayashi et al., 2009), NGC 1569 (Westmoquette et al., 2008),

NGC 3079 (Cecil et al., 2001). Hence, many questions, particularly those related to the GW in dwarf galaxies, remain open. Depending on the wind energy and the mass of the galaxy itself, matter can be both swept out into the intergalactic medium and, not possessing a sufficient initial velocity, get back to the galactic disk. In which cases is one or the other scenario realized? This requires both detailed theoretical calculations for specific objects (see, e.g., Melioli et al., 2013) and new observational data.

The NGC 4460 galaxy considered in this paper is a good “testing ground” for this kind of research. This is a dwarf lenticular galaxy with no noticeable companions, located in the scattered Canes Venatici cloud. According to the database of the Local Volume galaxies (Kaisina et al., 2012), its absolute magnitude is $M_B = -17.73$, the total mass $M = 6.4 \times 10^9 M_\odot$, and the accepted distance to it amounts to 9.59 Mpc, which gives an apparent scale of about 47 pc/arcsec.

An extended emission nebula was discovered here within the H α -survey of nearby galaxies (Kaisin & Karachentsev, 2008). Its spectroscopic study is presented in Moiseev et al. (2010). It has been shown that most of the emission line radiation originates from the compact (with a diameter of about 1 kpc) region in the galactic disk center, which is also confirmed by the optical (HST, SDSS) and ultraviolet (GALEX) images. At the same time, diffuse radiation in the H α line is distributed along the axis of rotation of the galaxy on both sides of the nucleus over long distances (up to 1.5 kpc). Ionization of gas in these areas is due to the combined influence of photoionization of young hot stars and shock waves related to current star formation. This

Send offprint requests to: *D. Oparin e-mail: doparin@mail.ru

*** A. Moiseev e-mail: moisav@gmail.com

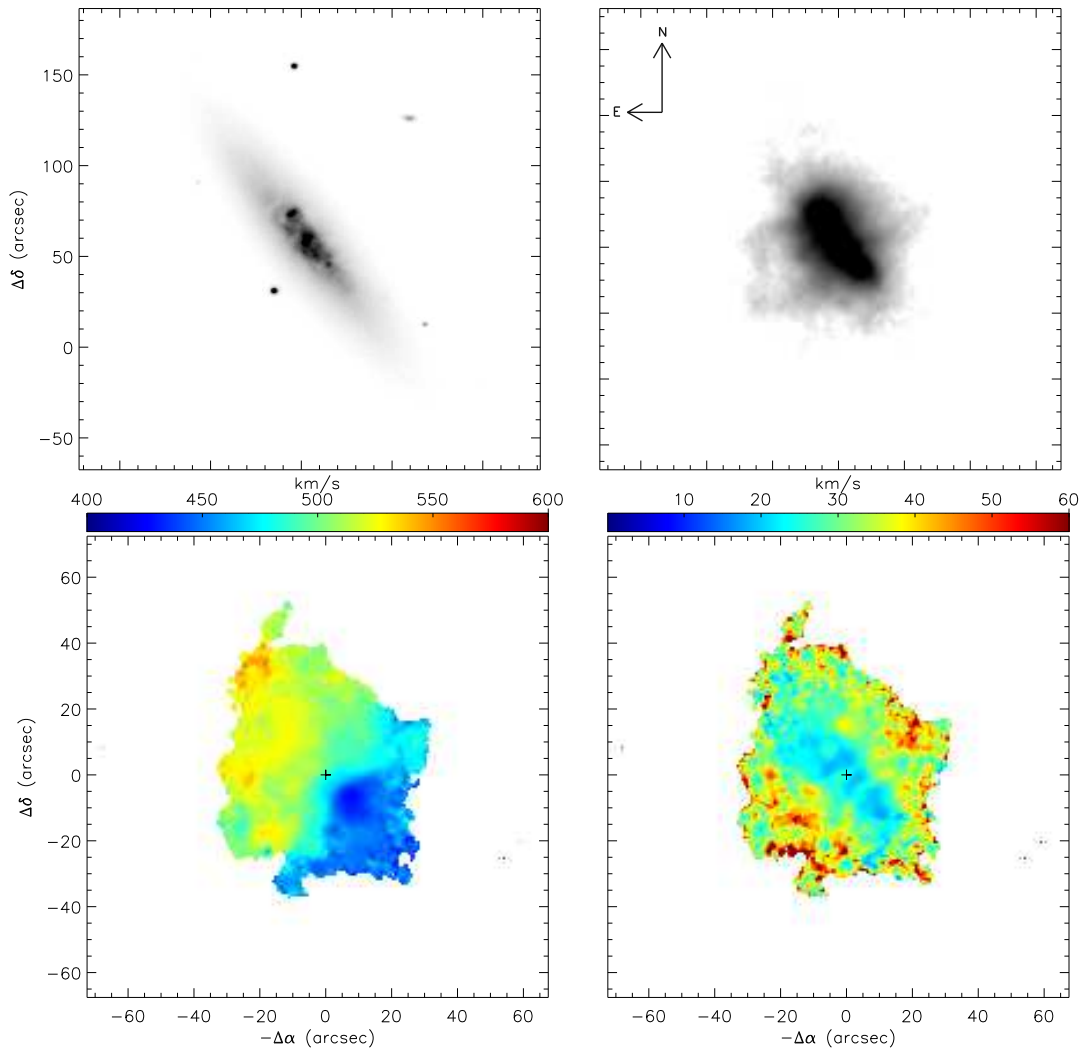


Fig. 1. Top left: an SDSS image of the NGC 4460 galaxy in the r filter; top right: an image in the emission $H\alpha$ line. Bottom left: the velocity field; bottom right: the line-of-sight velocity dispersion field.

way, according to Moiseev et al. (2010), the extended nebula in NGC 4460 is generated by the galactic wind. The outflow velocity estimates made in the same study amounted to more than 130 km s^{-1} , the kinetic energy of the wind was found to be $5.8 \times 10^{52} \text{ erg}$, and the characteristic time of formation of the observed structure amounted to 10–12 Myr.

The data on the motions of ionized gas in the GW region was provided in Moiseev et al. (2010) based on only two spectral cross sections with a resolution corresponding to $\text{FWHM} \approx 110 \text{ km s}^{-1}$ in the $H\alpha$ line, the central kiloparsec region was also observed with a panoramic spectrograph with a resolution $\text{FWHM} \approx 160 \text{ km s}^{-1}$. That was enough to measure the ionization state of the gas. However, higher resolution in line-of-sight velocity for the largest possible number of emitting regions is desirable for a detailed study of kinematics of the galactic wind. This

was done in this paper based on the observations with a scanning Fabry–Perot interferometer (FPI).

2. OBSERVATIONS AND DATA REDUCTION

The observations were made on May 19 and 20, 2010 on the 6-m telescope of the Special Astrophysical Observatory of the Russian Academy of Sciences (SAO RAS) with a scanning FPI installed inside the focal reducer SCORPIO (Afanasiev & Moiseev, 2005) in the $H\alpha$ line with an average seeing of $2''.5$. The IFP751 interferometer at the given wavelength provided a free spectral range $\Delta\lambda = 8.7 \text{ \AA}$ between the adjacent interference orders and a spectral resolution of 0.4 \AA (19 km s^{-1}) at a scale of 0.21 \AA per channel. The operating band around the redshifted $H\alpha$ line was separated by a narrowband filter.

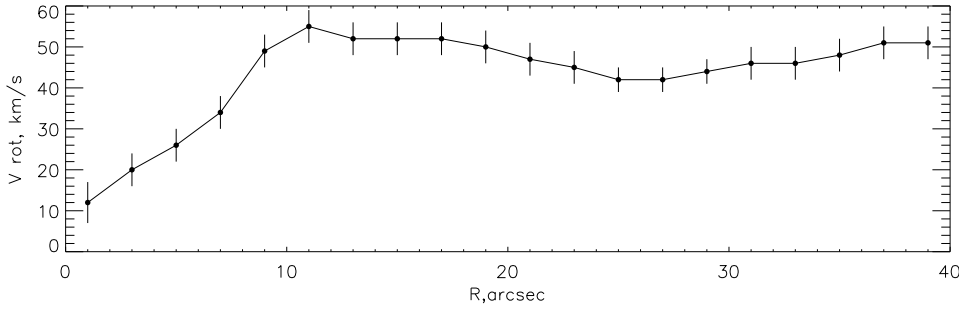


Fig. 2. Rotation curve of the galaxy.

Scanning consisted of a series of 40 interferograms (two 40×80 -s series) obtained with different distances between the interferometer plates, evenly filling the spectral range. The result of data reduction, conducted with an application package running in the IDL environment (Moiseev, 2002; Moiseev & Egorov, 2008), is a data cube, where each pixel contains a 40-channel spectrum.

As a result of approximation of the $H\alpha$ emission line profiles by the Voigt function, we built the images in the $H\alpha$ line and in the continuum as well as the line-of-sight velocity and velocity dispersion maps (Fig. 1).

3. ANALYSIS OF THE LINE-OF-SIGHT VELOCITY DISTRIBUTION

3.1. Galactic Disk Rotation Model

The ionized gas velocity field derived from the observations with the FPI has already been used in (Moiseev, 2014) to obtain an average rotation curve of the galaxy. Interestingly, even outside the plane of the disk, in the GW region, the line-of-sight velocity distribution is dominated by the component corresponding to circular rotation. Apart from the stellar wind, the rotation of the galaxy itself also contributes to the line-of-sight velocity of each point of the galaxy. Therefore, to eliminate it, we had to create a model of circular rotation and then subtract it from the velocity field. The rotation model was built by the tilted-ring model under the assumption of a flat thin disk (see (Moiseev, 2014) for details).

The following parameters, adopted from Moiseev et al. (2010), were used to construct the rotation model:

$PA_0 = 42^\circ \pm 2^\circ$, the position angle of the line of nodes;

$V_{\text{sys}} = 487 \pm 1 \text{ km s}^{-1}$, the systemic velocity;

$i = 77^\circ$, the angle between the sky plane and the plane of the galactic disk.

The rotation curve of the galactic disk, obtained from the velocity field is shown in Fig. 2. In the following section we extrapolate this rotation curve to the region occupied by the galactic wind.

3.2. Wind Cone Modeling

The outflow from the region of active star formation takes place in directions perpendicular to the plane of the galaxy, as the matter density in this direction is substantially lower than in the equatorial plane. Thus, there occurs an “emersion” of the expanding swept-out shell into a less dense environment, as is the case in the galaxies explored in detail, such as NGC 1482, NGC 3079, or M 82 (see the references in the Introduction). The observed velocity field is dominated by circular rotation. This indicates that the swept-out matter does not meet any serious resistance. It can hence be assumed that its rotation moment is maintained. Based on the above, we can build a model of rotation of the ejected shells.

We have assumed that the matter ejected from the active star formation region outflows as one large structure—a shell. Such a shell can be approximated by a frustum of a cone whose axis passes through the galactic center and the smaller base is located in the galactic disk. Here, only the walls of this cone could basically be observed in the $H\alpha$ line, while the hot gas inside does not radiate in the Balmer emission lines. It is worth noting that these walls do not absolutely have to be continuous, since in other galaxies with GW, the cones emitting in optical lines usually consist of separate filaments formed under the effect of various kinds of instabilities (Veilleux et al., 2005). Several such filaments are also visible in the $H\alpha$ image of NGC 4460.

The opening angle of the cone is assumed to be 60° , which describes the observed structure quite well.

When modeling the cone, we assumed that the outflowing matter is not experiencing any significant rotation velocity losses, since the rotation moment is preserved (see above), and the matter is not ejected from the nucleus itself but from an extended kiloparsec area, and hence the radial motion from the axis of rotation is not substantial. Within this assumption, the contribution of rotation in line-of-sight velocity is not dependent on which side of the cone we observe, whether it is the closest or the farthest to us, and which of the cones is closer to us.

Rotation velocities of the cone are taken according to the accepted rotation curve (Fig. 2). The inclination angle

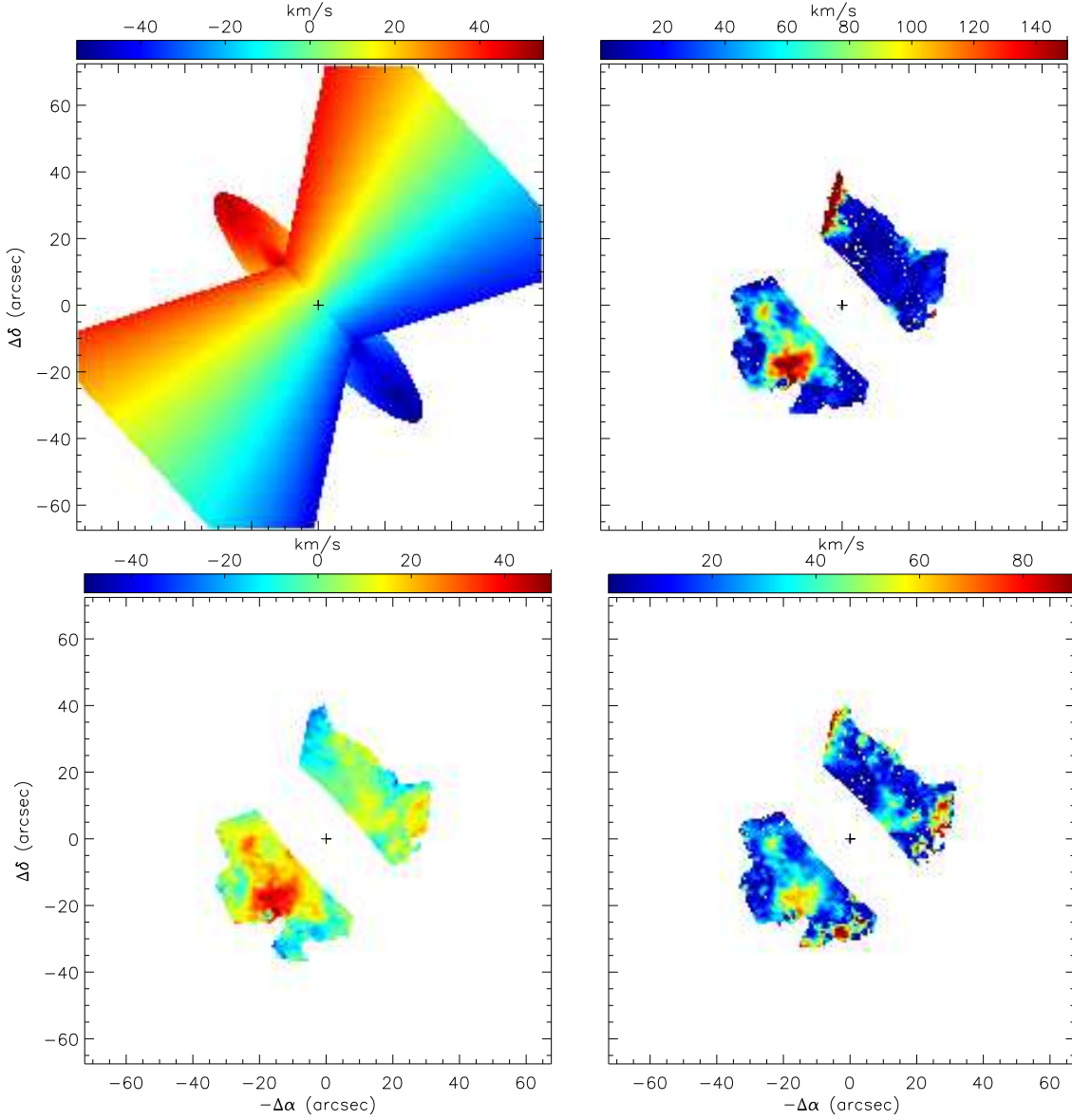


Fig. 3. Top left: a model of rotation of the galactic disk and swept-out matter of the galactic wind; bottom left: the map of residual velocities, the central regions are masked. Top right: the swept-out matter velocity map along the walls of the cone (the projection effect is taken into account) for the case when the southeast cone is closer to the observer; bottom right: a similar map for the case when the northwest cone is closer to the observer. We believe the last orientation to be the most plausible.

of the galaxy is $i = 77^\circ$; notice that it is difficult to determine the disk orientation relative to the observer based on direct images.

3.3. Residual Velocities

Subtraction of the wind rotation model from the velocity field produces the map of residual velocities, shown in Fig. 3 (bottom left). We can see no significant velocity gradients in the direction of rotation, which allows to consider our suggestion on small differences between the

rotation velocities in the disk and wind to be adequate enough.

Since the axis of rotation of the galaxy is inclined from the sky plane by only 13° , and assuming that the entire gas observed in the cones belongs to the walls and moves only in the direction from the disk, we can assert that the negative residual line-of-sight velocity supposes the motion on the wall of the cone closest to us, while the positive velocity would imply the farthest wall. The region where this rule would not work, as the sections of both walls of the cone is on the same side of the sky plane, is less than ten percent of the cone radius at that point, namely,

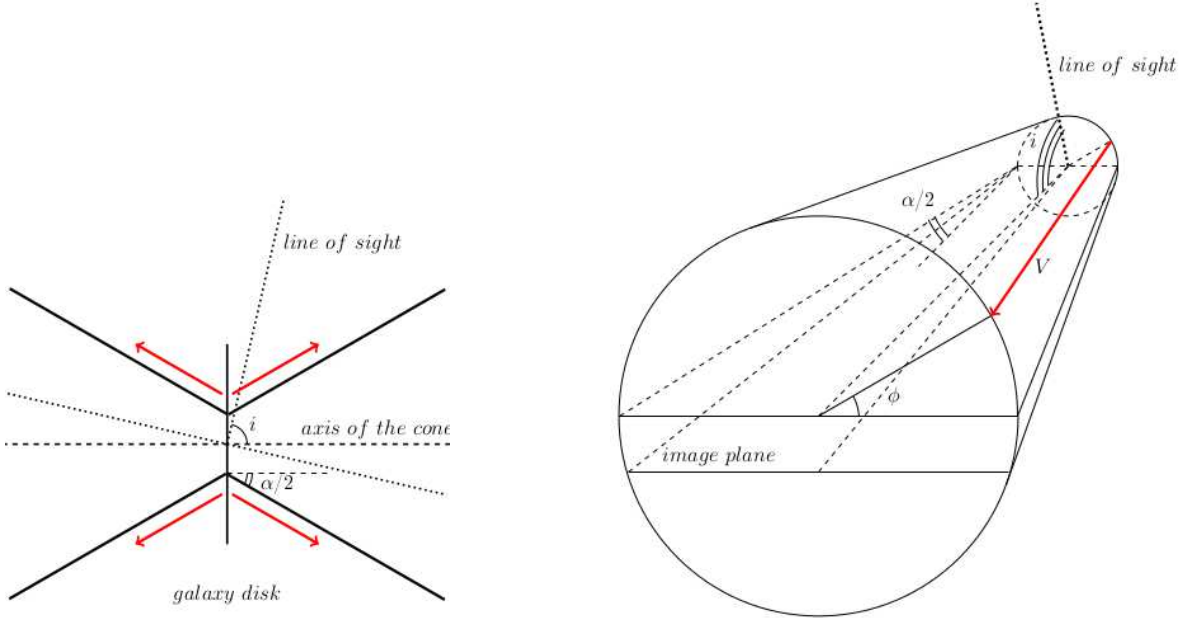


Fig. 4. Scheme of gas motion in the cone depending on the spatial location. Left: the view from the plane perpendicular to the disk of the galaxy; right: the view from the side of the cone axis. The line of sight shows the direction to the observer. We can see that if the ϕ angle is sufficiently small, i.e., the point lies close to the visible boundary of the cone, then for both its possible positions (on the near and far walls of the cone from the observer) the outflow velocity vectors will be directed to one side from the sky plane.

within two to three pixels at the edges of the cone (Fig. 4). Thus, after subtracting the model of rotation and systemic velocity, we can determine the spatial distribution of gas emitting in H α as well as on the velocities of its rotation.

The calculation of velocities is carried out according to the formula derived from simple geometric considerations (Fig. 4):

$$V_{\text{out}} = \frac{V_{\text{res}}}{\cos(\alpha/2) \cos i + \sin(\alpha/2) \sin i \sin \phi},$$

where V_{out} is the sought velocity of gas moving along the cone walls, V_{res} is the residual line-of-sight velocity after subtracting the circular component, i is the angle between the sky plane and the plane of the galactic disk, $\alpha/2$ is the half opening angle of the cone projection, ϕ is the azimuth angle relative to the axis of the cone.

Because of uncertainty of the spatial orientation of the galactic axis, it is not safe to say which of the model cones is closer to the observer, which is required to recalculate the residual line-of-sight velocities into the gas motion velocities along the walls of the cone. We will hence consider both variants of cone orientation. Apart from that, due to the effect of projection on the picture plane, there occurs an uncertainty whether the radiating point is located in the near or far wall of the cone relative to the observer. This uncertainty affects the ϕ angle. However, as we noted above, knowing the sign of residual line-of-sight velocities, we can deduce on which side of the cone the emitting point is located.

Having accounted for the projection effect, we get that the model in which the southeast cone is accepted to be

located closer to the observer has a clearly different distribution of wind velocities on both sides of the galaxy: 130–150 km s⁻¹ for the southeast and 10–30 km s⁻¹ for the northwest cones; while the second model (where the southeast cone is taken to be the farthest from the observer) gives much closer outflow velocities for both cones. Therefore, further on we accept this spatial orientation. The high-velocity regions at the cone boundaries are of little use for the analysis, as here we cannot clearly identify to which side, near or far, the matter belongs, which means that we cannot calculate the ϕ angle, and also due to the difference of our simple model from the real morphology of the wind, which leads to obviously false results at small $|\sin(\phi)|$ values.

4. DISCUSSION

4.1. Wind Parameters. Comparison with Other Galaxies

The constructed outflow velocity map (Fig. 3, bottom right) reveals individual rapidly moving filaments on the background of relatively slow gas, $V_{\text{out}} = 10\text{--}20$ km s⁻¹. Figure 5 gives the histograms of velocity distribution within such regions. The analysis of these histograms allows us to conclude that the characteristic velocities of the galactic wind in NGC 4460 range within 30–80 km s⁻¹.

When compared to other galaxies, such as NGC 1482 where outflow velocities reach 250 km s⁻¹ (Veilleux & Rupke, 2002), or 300–350 km s⁻¹

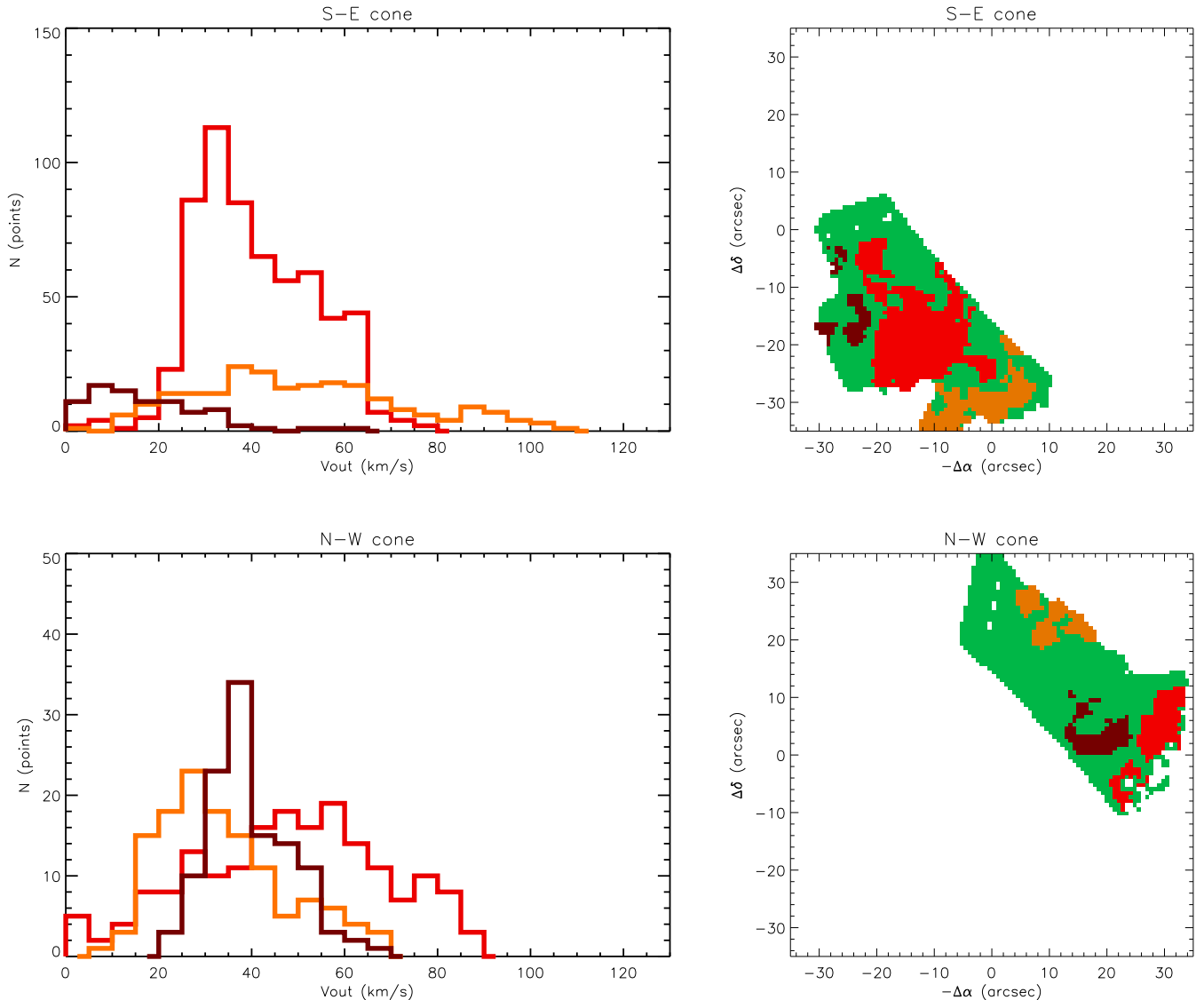


Fig. 5. Velocity distribution in the fastest filaments for the far (southeastern, at the top) and near (northwestern, at the bottom) cones. Right: locations of the considered filaments on the sky plane; left: the histogram of velocity distribution in them. Green regions—background areas with low ($10\text{--}20\text{ km s}^{-1}$) velocities—are not represented in the histogram. Colors mark local areas with high velocities of motion along the cone walls.

in M82 (Westmoquette et al., 2009), the wind in NGC 4460 shows significantly lower velocities, comparable with the outflows in dwarf galaxies, such as NGC 2366 ($30\text{--}50\text{ km s}^{-1}$ —van Eymeren et al., 2009A) or NGC 4681 ($30\text{--}80\text{ km s}^{-1}$ —van Eymeren et al., 2009B). Notice that in contrast to these two galaxies, where individual isolated outflows from HII regions were observed, a much more large-scale and collimated structure of galactic wind is present in NGC 4460.

Based on the line widths measured in the low-resolution spectra, a wind velocity estimate of more than 130 km s^{-1} has previously been obtained in Moiseev et al. (2010). Now we have substantially refined this parameter, as our geometric model allowed us to confidently separate

the component corresponding to the GW in the velocity field. This allowed us to adjust the values of other wind parameters: the age of the structure formed by the wind lies within $20\text{--}50\text{ Myr}$; at the mass of gas ejected from the disk $M_{\text{wind}} = 1.7 \times 10^5 M_{\odot}$, its kinetic energy would be $E_{\text{wind}} = 0.3\text{--}2.2 \times 10^{52}\text{ erg}$.

The distribution of the line-of-sight velocity dispersion perpendicularly to the galactic disk (Fig. 6) shows that turbulent motions in gas become substantial outside the bright dense regions: velocity dispersion values there reach $40\text{--}50\text{ km s}^{-1}$, which is comparable with the outflow velocity itself, according to our estimates. Notice that a small contribution to the measured velocity dispersion is brought in by the thermal broadening of emission lines, it

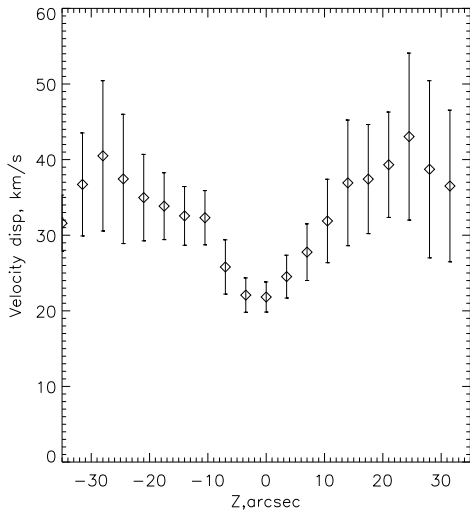


Fig. 6. Dependence of the velocity dispersion on the distance to the galactic disk and the outflow velocity.

amounts to about 10 km s^{-1} for an electron temperature of about 10 000 K, typical for the H II regions.

4.2. The Galaxy Escape Velocity

Using a procedure similar to that discussed by van Eymeren et al. (2009A,B), we try to determine whether the wind velocity is sufficient to overcome the galactic gravity and allow the gas to be ejected into intergalactic space.

To estimate the velocity required for gas to leave the galaxy, let us use the model of a spherical pseudo-isothermal dark matter halo, which describes well the outer curves of rotation for dwarf galaxies.

In this model, the galaxy escape velocity is

$$V_{\text{esc}}(r) = \sqrt{2V_c^2(1 + \ln(r_h/r))},$$

where V_c is the rotation velocity of the galaxy, r_h is the dark halo radius (Binney & Tremaine, 1987).

We assume the radius of the halo to be equal to the Holmberg radius of the galaxy of 2'1 (Kaisina et al., 2012), which is about 6 kpc.

The diagram of the velocity distribution of matter outflow depending on the distance to the galactic center, is shown in Fig. 7. If we impose on it the curve of the model galaxy-escape velocity, we can see that the bulk of matter is located considerably lower, i.e., it does not reach these velocities. Several points formally located above the $V_{\text{esc}}(r)$ line are most likely due to the errors caused by a different direction of the velocity vector than that expected in Section 3.3.

Therefore, the outflow of matter occurs with velocity insufficient to escape the galaxy.

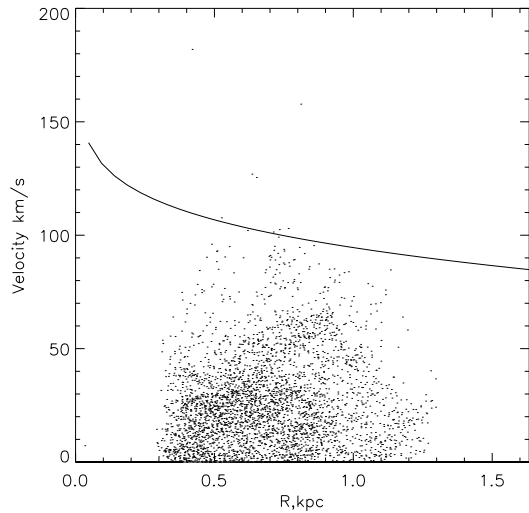


Fig. 7. Velocity distribution of the matter outflow from the plane of the galactic disk (dots) depending on the distance to the galactic center. The solid line represents the dependence of the velocity required for the matter to escape from the galaxy in the model of a pseudo-isothermal halo with a radius of 6 kpc.

5. CONCLUSION

The observations with a scanning Fabry–Perot interferometer with a sufficiently high spectral (about 19 km s^{-1}) and spatial (about 120 pc) resolution allowed us to study the structure of the galactic wind in NGC 4460:

- the galactic wind in NGC 4460 is mainly represented by two streams outflowing from the galactic disk plane in opposite directions; typical velocities of these streams are $30\text{--}80 \text{ km s}^{-1}$;
- the galactic wind in NGC 4460 is a ragged, very perturbed, and complex structure.

A comparison of the velocities of galactic wind and the model escape velocities for the case of pseudo-isothermal dark matter halo suggests that the wind energy is not strong enough to eject the gas beyond the galactic gravitational well. Therefore, we expect that over time, having cooled down, the matter will again infall onto the galactic disk. This finding is consistent with the similar results of van Eymeren et al. (2009A,B), obtained for local outflows of ionized gas in NGC 2366 and NGC 4681.

Acknowledgements. The work was supported by grant No. 14-22-00041 of the Russian Science Foundation. The article is based on the data of observations carried out on the SAO RAS 6-m telescope with financial support by the Ministry of Education and Science of the Russian Federation (agreement No. 14.619.21.0004, project ID PRFMFI61914X0004).

References

Arribas S., Colina L., Bellocchi E., et al., 2014, *A&A*, 568,

A14

- Afanasiev V. L. and Moiseev A. V., 2005, *Astronomy Letters*, 31, 194
- Binney J. and Tremaine S., *Galactic Dynamics* (Princeton Univ. Press, Princeton, 1987).
- Cecil G., Bland-Hawthorn J., Veilleux S., and A. V. Filippenko., 2001, *ApJ*, 555, 338
- Hopkins P. F., Quataert E., and Murray N., 2012, *MNRAS*, 421, 3522
- Kaisin S. S. and Karachentsev I. D., 2008, *A&A*, 479, 603
- Kaisina E. I., Makarov D. I., Karachentsev I. D. and Kaisin S. S., 2012, *Astrophysical Bulletin*, 67, 115
- Matsubayashi K., Sugai H., Hattori T., et al., 2009, *ApJ*, 701, 1636
- C. Melioli, E. M.de Gouveia Dal Pino, and F. G. Geraissate, 2013, *MNRAS*, 430, 3235
- Moiseev A. V., 2002, *Bull. Spec. Astrophys. Obs.* , 54, 74
- Moiseev A. V., 2014, *Astrophysical Bulletin*, 69, 1
- Moiseev A. V. and Egorov O. V., 2008, *Astrophysical Bulletin*, 63, 181
- Moiseev A. V., Karachentsev I. D., and Kaisin S. S., 2010, *MNRAS*, 403, 1849
- Pettini M., Kellogg M., Steidel C. C., et al., 1998, *ApJ*, 508, 539
- van Eymeren J., Marcelin M., Koribalski B., et al., 2009A, *A&A* , 493, 511
- van Eymeren J., Marcelin M., Koribalski B., et al., 2009B, *A&A* , 505, 105 (2009).
- Veilleux S., Cecil G., Bland-Hawthorn J., 2005, *ARA&A*, 475, 479
- Veilleux S. and Rupke D. S., 2002, *ApJ*, 565, L63
- Westmoquette M. S., Smith L. J., and Gallagher J. S., 2008, *MNRAS*, 383, 864
- Westmoquette M. S., Smith L. J., Gallagher III J. S., et al., 2009, *ApJ*, 696, 192